Crosstalk Noise in WDM-Based Optical Networks-on-Chip: A Formal Study and Comparison

Mahdi Nikdast, *Member, IEEE*, Jiang Xu, *Member, IEEE*, Luan Huu Kinh Duong, Xiaowen Wu, *Student Member, IEEE*, Xuan Wang, *Student Member, IEEE*, Zhehui Wang, Zhe Wang, Peng Yang, Yaoyao Ye, and Qinfen Hao

***Abstract*— Optical networks-on-chip (ONoCs) using wavelength-division multiplexing (WDM) technology have progressively attracted more and more attention for their use in tackling the high-power consumption and low bandwidth issues in growing metallic interconnection networks in multiprocessor systems-on-chip. However, the basic optical devices employed to construct WDM-based ONoCs are imperfect and suffer from inevitable power loss and crosstalk noise. Furthermore, when employing WDM, optical signals of various wavelengths can interfere with each other through different optical switching elements within the network, creating crosstalk noise. As a result, the crosstalk noise in large-scale WDM-based ONoCs accumulates and causes severe performance degradation, restricts the network scalability, and considerably attenuates the signal-to-noise ratio (SNR). In this paper, we systematically study and compare the worst case as well as the average crosstalk noise and SNR in three well-known optical interconnect architectures, mesh-based, folded-torus-based, and fat-tree-based ONoCs using WDM. The analytical models for the worst case and the average crosstalk noise and SNR in the different architectures are presented. Furthermore, the proposed analytical models are integrated into a newly developed crosstalk noise and loss analysis platform (CLAP) to analyze the crosstalk noise and SNR in WDM-based ONoCs of any network size using an arbitrary optical router. Utilizing CLAP, we compare the worst case as well as the average crosstalk noise and SNR in different WDM-based ONoC architectures. Furthermore, we indicate how the SNR changes in respect to variations in the number of optical wavelengths in use, the free-spectral range, and the microresonators Q factor. The analyses' results demonstrate that the crosstalk noise is of critical concern to WDM-based ONoCs: in the worst case, the crosstalk noise power exceeds the signal power in all three WDM-based ONoC architectures, even when the number of processor cores is small, e.g., 64.**

***Index Terms*— Optical crosstalk noise, optical interconnects, optical losses, signal-to-noise ratio (SNR), wavelength-division multiplexing (WDM).**

I. Introduction

ON-CHIP communication in multiprocessor systems-on-chip (MPSoCs) is rapidly growing due to the integration of many processor cores on a single die. Networks-on-chip (NoCs) can bring better scalability and performance to the traditional communication infrastructure in MPSoCs. However, as the technology continues to scale down and allows integration of an even larger number of processor cores, the metallic interconnects' power dissipation in NoCs will progressively increase to a considerable portion of the system power budget, becoming a bottleneck. On-chip optical communication and integration technologies, however, present an appealing solution for outperforming the low bandwidth, high latency, and high-power dissipating metallic interconnects in MPSoCs. Furthermore, the employment of wavelength-division multiplexing (WDM) technology in optical NoCs (ONoCs) can further boost the bandwidth in optical interconnects through concurrent transmission of multiple optical signals on a single waveguide.

Several optical NoCs employing WDM with high-capacity and low-power consumption have been proposed based on mesh, torus, and fat-tree topologies, in which optical waveguides and microresonators (MRs) are extensively used [2]–[4]. These basic photonic devices, however, suffer from inevitable crosstalk noise and power loss. Some components in WDM-based ONoCs, such as filters, wavelength multiplexers/demultiplexers, switches, and semiconductor optical amplifiers, introduce interchannel and intrachannel crosstalk noise. Interchannel crosstalk noise occurs when the crosstalk signal is at a wavelength different from the desired signal's wavelength, while intrachannel crosstalk noise occurs when the crosstalk signal is at the same wavelength as that of the desired signal or sufficiently close to it. Intrachannel crosstalk effects can be much more severe than those of interchannel crosstalk since they cannot be removed by filtering [5]. In this paper, we focus on analyzing first-order incoherent interchannel and intrachannel crosstalk noise, and for convenience, we use crosstalk noise when referring to the two types in the rest of this paper. In large-scale WDM-based ONoCs, the crosstalk noise from the basic photonic devices in the optical switching elements and from the interferences among the different wavelengths in the WDM-based network accumulates on the optical signal in question and eventually diminishes the signal-to-noise ratio (SNR) as well as imposes scalability constraints. The SNR determines the feasibility of WDM-based ONoCs, and thus it is essential to find and analyze the worst case and the average SNR in different WDM-based ONoCs. In addition, the analysis of crosstalk noise and SNR is topology dependent and is different in

Manuscript received April 1, 2014; revised August 18, 2014; accepted October 21, 2014. This work was supported by Huawei Technologies Company, Ltd.

M. Nikdast, J. Xu, L. H. K. Duong, X. Wu, X. Wang, Z. Wang, Z. Wang, and P. Yang are with the Department of Electronic and Computer Engineering, Hong Kong University of Science and Technology, Hong Kong (e-mail: mnikdast@connect.ust.hk; jiang.xu@ust.hk).

Y. Ye and Q. Hao are with Huawei Technologies Company, Ltd., Shenzhen 518129, China.

Color versions of one or more of the figures in this paper are available online at http://ieeexplore.ieee.org.

Digital Object Identifier 10.1109/TVLSI.2014.2370892

various WDM-based ONoC architectures, necessitating the development of a unique approach for each architecture to realize the SNR analysis in that architecture.

The worst case crosstalk noise and SNR in arbitrary mesh-based, folded-torus-based, and fat-tree-based ONoCs were analyzed in [6]–[8]. The proposed formal analytical models at the device, router, and network levels in those works are based on the consideration of a single wavelength only, and hence cannot consider the impact of the interchannel and intrachannel crosstalk noise existing in WDM-based networks. Moreover, they only consider the worst case crosstalk noise and SNR analyses; however, the average analyses are also of vital importance. In addition, Duong *et al.* [9] presented an analysis of the worst case SNR specifically for a case study of WDM-based ring-based ONoCs, the corona network.

The novel contribution of this paper is presenting a systematic study and comparison of the worst case as well as the average crosstalk noise, power loss, and SNR in mesh-based, folded-torus-based, and fat-tree-based ONoCs using WDM. We present formal analyses for real case studies of WDM-based mesh-based and WDM-based folded-torus-based ONoCs using the Crux optical router and WDM-based fat-tree-based ONoCs using the optical turn-around router (OTAR). Moreover, the newly developed crosstalk and loss analysis platform (CLAP), presented in [7], has been upgraded by including the proposed formal analytical models for the worst case and the average crosstalk noise and SNR in arbitrary WDM-based ONoCs. The proposed analytical models for modulators and photodectors as well as the fat-tree topology are also included in CLAP. The analyses start hierarchically from the basic photonic device level, to the optical router level, and finally, to the network level. Therefore, the analytical models at the network level can be easily translated into the initial device level models for validation. The analytical models proposed for the basic optical elements can be applied to any WDM-based ONoC. Utilizing the proposed analyses, CLAP, and considering recent photonic device parameters, we present a detailed study and comparison of the worst case and the average crosstalk noise power, signal power, and SNR in WDM-based mesh-based, folded-torus-based, and fat-tree-based ONoCs. The quantitative simulation results signify the severe effect of crosstalk noise in WDM-based ONoCs: the worst case and the average SNR decrease exponentially in WDM-based ONoCs as the network scales. Furthermore, the SNR in WDM-based ONoCs is reversely related to the number of employed optical wavelengths in the network: the SNR drops quickly as the number of optical wavelengths in use increases over a fixed free-spectral range (FSR).

We analyze mesh-based and folded-torus-based ONoCs of a hybrid structure consisting of a packet-switched electronic network, for controlling the photonic network and routing control packets, and a circuit-switched photonic network, which is responsible for transmitting the payload data. The fat-tree-based ONoC is a hierarchical, multistage network in which payload data and network control data are both being transmitted on the same optical network. An off-chip vertical cavity surface emitting laser (VCSEL) is considered as the laser source. Dimension-ordered routing is used in the mesh-based and folded-torus-based networks, while the optical turnaround routing algorithm is considered in the fat-tree-based networks. Analyses of dynamic variations in optical devices, such as laser and thermal noise, as well as fabrication variations are not considered in this paper.

The rest of this paper is organized as follows. Section II summarizes some of the related works. Section III describes detailed analyses of the basic optical elements and optical routers used in WDM-based ONoCs. We present the worst case as well as the average crosstalk noise and SNR analyses at the network level in Section IV. Section V presents the quantitative simulation results and comparisons. Finally, the conclusion is drawn in Section VI.

II. Related Works

Although there are several works that have tackled the crosstalk noise issue at the device level [10]–[12], only a few works have explored it at the network level in ONoCs. Xie *et al.* [13] studied the worst case crosstalk noise and SNR in mesh-based ONoCs using an optimized optical crossbar router. In the same work, it was proved that the worst case SNR link is not always the longest optical link, which suffers from the highest power loss in the network. Moreover, a compact high-SNR optical router, called the Crux optical router, was proposed to improve the SNR of ONoCs. The same group systematically analyzed the worst case crosstalk noise and SNR in general mesh-based ONoCs using an arbitrary optical router in [6]. In addition, Nikdast *et al.* [7], [8] proposed formal analytical approaches to analyze the worst case crosstalk noise and SNR in folded-torus-based and fat-tree-based ONoCs using arbitrary optical routers. The ONoC considered in all the aforementioned works utilizes a single-wavelength approach.

Chan *et al.* [14] proposed a methodology to characterize and model basic photonic blocks, which can form full photonic network architectures, and used a physical-layer simulator to assess the physical-layer and system-level performance of a photonic network. Vaez and Lea [15] indicated that the crosstalk noise is an intrinsic, serious issue in directional-coupler-based optical networks, and Lin and Lea [16] developed an analytical model to characterize the crosstalk noise level in a microring-based optical interconnection network. The fundamental limits for the number of WDM channels and power per channel when using building blocks that include silicon waveguides, silicon microring modulators, and filters were described in [17].

III. Basic Optical Elements and Optical Routers in WDM-Based ONoCs

Almost every component in WDM-based ONoCs introduces crosstalk noise. Among these components, those presented and studied in this paper have the highest impact on the worst case and the average SNR in WDM-based ONOCs. Waveguides and MRs are the two fundamental optical elements employed to construct basic optical switching elements (BOSEs) and optical routers. Optical routers consist of BOSEs, waveguide

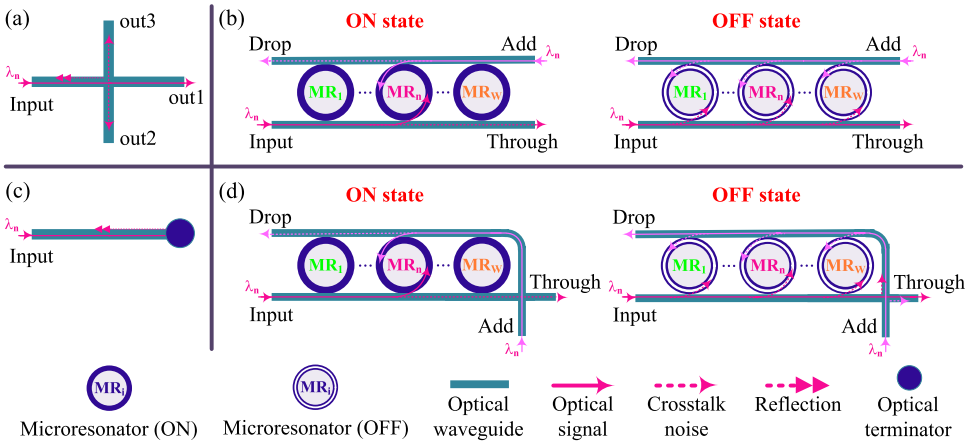

Fig. 1. Basic optical elements and BOSEs: (a) Waveguide crossing, (b) PSE in ON and OFF states, (c) Optical terminator, and (d) CSE in ON and OFF states.

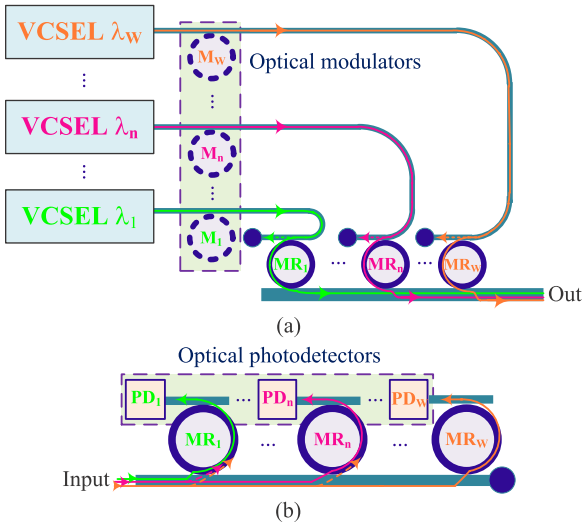

Fig. 2. (a) Optical modulator, and (b) photodetector models as a part of the E-O and O-E interfaces.

crossings, waveguide bendings, and optical terminators. The waveguide crossing, shown in Fig. 1(a), is a structure consisting of two crossed orthogonal waveguides. Two types of basic 1×2 optical switching elements are the parallel switching element (PSE) and the crossing switching element (CSE). The PSE consists of an MR located between two parallel waveguides, as shown in Fig. 1(b). The optical terminator, shown in Fig. 1(c), is responsible for absorbing the optical signal at the input port and then avoiding it reflecting back onto the input port. The structure shown in Fig. 1(d), consisting of an MR adjacently positioned next to a waveguide crossing intersection, is the CSE.

WDM-based ONoCs also include optical modulators and photodetectors in their electronic-optical (E-O) and optical-electronic (O-E) interfaces. The optical modulator as a part of the E-O interface is responsible for modulating the optical signal by an information data signal at the very beginning of any on-chip optical communication. In this paper, we consider external modulation, in which the optical signal is modulated after its generation at the laser source. The optical photodetector as a part of the O-E interface is employed to detect the modulated optical signal at the end of the communication line at the receiver. Fig. 2 shows the optical modulators and photodetectors in WDM-based ONoCs. We consider an active MR-based switching technique, in which the MRs can be powered ON (the ON state) or OFF (the OFF state) by applying an electrical voltage to the p-n contacts surrounding the ring.

We analyze and model the power loss and crosstalk noise in basic optical devices and later in optical routers in WDM-based ONoCs in this section. Table I lists the notations and their recent values considered for power loss, crosstalk noise, and reflectance coefficients in basic optical elements [11], [14], [18]–[20]. It is worth mentioning that the proposed analytical models in this paper are based on the defined notations, and hence the power loss and coefficient values listed in Table I are used only as an example.

TABLE I
POWER LOSS VALUES, CROSSTALK NOISE, AND REFLECTANCE COEFFICIENTS

Notation	Definition	Value
L_c	Crossing loss	-0.04 dB
L_p	Propagation loss per cm	-0.274 dB/cm
L_b	Bending loss	-0.005 dB/90°
L_{p0}	Average passing loss per MR in OFF state	-0.005 dB
L_{p1}	Average drop loss per MR in ON state	-0.5 dB
L_m	Average modulation loss	-0.005 dB
K_c	Crossing's crosstalk	-40 dB
K_r	Crossing's back-reflection	$\cong 0$
K_{p0}	Crosstalk per MR in OFF state	-20 dB
K_{p1}	Crosstalk per MR in ON state	-25 dB
K_t	Optical terminator's reflectance	-50 dB

A. Analytical Models for Basic Elements

Considering the waveguide crossing in Fig. 1(a), the input optical signal of the wavelength λ_n passes the crossing intersection with some insertion loss at the out1 output port,

while there is a portion of the signal power which goes to the out2 and out3 output ports and also reflects back on the input port. Given $P_{\text{in}}^{\lambda_n}$ as the power of the optical signal at the input port, (1) calculates the output powers at the out1, out2, and out3 output ports, $P_{\text{out1}}^{\lambda_n}$, $P_{\text{out2}}^{\lambda_n}$, and $P_{\text{out3}}^{\lambda_n}$, as well as the reflected power, $P_{Rc}^{\lambda_n}$, on the input port in the waveguide crossing. In (1) and also the rest of the equations in this paper, n is the number of the optical wavelength under study and $n \in [1, W]$, where W is the total number of wavelengths considered in the network. In addition, λ_n indicates the wavelength number and is not an exponent

$$P_{\text{Out1}}^{\lambda_n} = L_c P_{\text{in}}^{\lambda_n} \tag{1a}$$

$$P_{\text{Out2}}^{\lambda_n} = P_{\text{Out3}}^{\lambda_n} = K_c P_{\text{in}}^{\lambda_n} \tag{1b}$$

$$P_{Rc}^{\lambda_n} = K_r P_{\text{in}}^{\lambda_n}. \tag{1c}$$

The main function of an optical terminator is to absorb the input light and prevent it from reflecting back onto the input port. A recent approach for terminating waveguides, considered in this paper, is through deeply etched gratings [20]. When an optical signal of the wavelength λ_n and with the optical power $P_{\text{in}}^{\lambda_n}$ enters an optical terminator, as shown in Fig. 1(c), the reflected power on the input port of the optical terminator can be defined as

$$P_R^{\lambda_n} = K_t P_{\text{in}}^{\lambda_n}. \tag{2}$$

Prior to studying the power loss and crosstalk noise in the PSE and CSE, we present an analytical model to characterize the interchannel and intrachannel crosstalk noise (see our discussion in Section I) in MR-based photonic switching elements. MRs have a lorentzian power transfer function, which is peaked at the resonant wavelength λ_{MR}. For optical signals carried on wavelength λ_n, the power transferred to the drop port can be expressed as (3a) [21]. In this equation, κ_e^2 and κ_e^2 are the fraction of the optical power that the lower waveguide and the upper waveguide couple into or out of the MR, respectively [Fig. 1(b)]. Moreover, κ_p^2 is the fraction of the intrinsic power losses per round trip in the MR. When $\kappa_d^2 + \kappa_e^2 \gg \kappa_p^2$, nearly full power transfer can be achieved at the peak resonance point, and the MR will exhibit a low insertion loss. Without loss of generality, we suppose that $\kappa_d^2 + \kappa_e^2 \gg \kappa_p^2$ and $\kappa_d = \kappa_e$. As a result, the coefficient before $\psi(n, \lambda_{\text{MR}m})$ in (3a) is equal to one

$$\frac{P_{\text{drop}}^{\lambda_n}}{P_{\text{in}}^{\lambda_n}} = \left(\frac{2\kappa_e\kappa_d}{\kappa_e^2 + \kappa_d^2 + \kappa_p^2}\right)^2 \cdot \psi(n, \lambda_{\text{MR}m}) \tag{3a}$$

where

$$\psi(n, \lambda_{\text{MR}m}) = \frac{\delta^2}{(\lambda_n - \lambda_{\text{MR}m})^2 + \delta^2}. \tag{3b}$$

In (3b), 2δ is the 3-dB bandwidth of the MR and it can be defined as $Q = (\lambda_{\text{MR}}/2\delta)$, in which Q is the quality factor of the MR. When an optical signal of the wavelength λ_n passes the MR m with the resonant wavelength $\lambda_{\text{MR}m}$ ($\lambda_n \neq \lambda_{\text{MR}m}$), a portion of the optical signal carried on λ_n couples into the ring and is directed to the drop port [Fig. 1(b)], generating crosstalk noise. According to (3b), the amount of this crosstalk noise is determined by the spacing between λ_n and $\lambda_{\text{MR}m}$ and the 3-dB bandwidth of the MR. In this paper, we suppose equal spacing among different optical wavelengths that cover a whole FSR. As a result, the spacing between the two consecutive wavelengths λ_n and λ_{n+1}, when the total number of wavelengths is W, equals (FSR/W). Therefore, for the optical signal of the wavelength λ_n, we have $\lambda_n = \lambda_0 + ((n-1)\text{FSR}/W)$. Similarly, for the MR$_m$, one can note that $\lambda_{\text{MR}m} = \lambda_{\text{MR}0} + ((m-1)\text{FSR}/W)$. In the former and latter equations, λ_0 and $\lambda_{\text{MR}0}$ can be decided by the system designer and we assume that $\lambda_0 = \lambda_{\text{MR}0}$.

Considering Fig. 1(b) and when the PSE is in the ON state, the input optical signal of the wavelength λ_n couples into the MR n, whose resonant wavelength is equal to λ_n ($\lambda_n = \lambda_{\text{MR}n}$), and makes a turn to the drop port, while a portion of the power goes to the through port as crosstalk noise. Please note that we only consider the first-order incoherent crosstalk noise in this paper, and hence when the PSE is in the ON state, the crosstalk noise from different wavelengths on the drop port is not considered. In addition, the two optical signals shown in Fig. 1(b) and (d) have the same optical wavelength of λ_n, but are from different power sources and hence incoherent. When an optical signal of the wavelength λ_n passes a PSE in the ON state, the output powers at the through, P_T, and drop, P_D, ports of the PSE are calculated in

$$P_{T\,\text{pse,ON}}^{\lambda_n} = K_{p1} L_{p0}^{W-1} P_{\text{in}}^{\lambda_n} \tag{4a}$$

$$P_{D\,\text{pse,ON}}^{\lambda_n} = L_{p0}^{2(n-1)} L_{p1} P_{\text{in}}^{\lambda_n}. \tag{4b}$$

According to Fig. 1(b), when the PSE is in the OFF state, the optical signal carried on the wavelength λ_n travels from the input port to the through port, while a portion of the signal (crosstalk noise) couples into the ring n, whose resonant wavelength is now shifted to the OFF state at $\lambda'_{\text{MR}n} = \lambda_{\text{MR}n} + \epsilon$ and $\epsilon < (\text{FSR}/W)$, and goes to the drop port. Furthermore, portions of the optical signals on the other wavelengths than λ_n, say λ_m where $m \in [1, W]$ and $n \neq m$, also couple into the ring n, creating crosstalk noise. When the PSE is in the OFF state, (5) calculates the output powers at the through and drop ports. As can be seen in this equation, for the optical signal of the wavelength λ_n passing the MR n in the OFF state, the crosstalk coefficient is assumed to be K_{p0}, as listed in Table I, since λ_n is the closest wavelength to $\lambda'_{\text{MR}n}$. However, (3b) helps calculate the crosstalk coefficient for the same optical signal passing other MRs than the ring n, whose resonant wavelengths are farther from λ_n. A similar assumption is considered in (4a) for using K_{p1} when the PSE is in the ON state. In addition, to simplify the analytical models, we assume the use of average passing and drop losses in the PSEs, L_{p0} and L_{p1} listed in Table I, for optical signals of different wavelengths and under different values of FSR and Q

$$P_{T\,\text{pse,OFF}}^{\lambda_n} = L_{p0}^{W} P_{\text{in}}^{\lambda_n} \tag{5a}$$

$$P_{D\,\text{pse,OFF}}^{\lambda_n} = K_{p0} L_{p0}^{2(n-1)} P_{\text{in}}^{\lambda_n} + \sum_{j=1, j\neq n}^{W} \left(L_{p0}^{2(j-1)} \psi\left(n, \lambda'_{\text{MR}\,j}\right)\right) P_{\text{in}}^{\lambda_n}. \tag{5b}$$

The CSE is composed of a waveguide crossing and a PSE. Leveraging the analytical models of the PSE and the waveguide crossing, we model the power loss and crosstalk noise in the CSE. Regarding Fig. 1(d), when the CSE is in the ON state, the output powers at the through and drop ports for an input optical signal of the wavelength λ_n are defined in

$$P_{T\,\mathrm{cse,ON}}^{\lambda_n} = K_{p1} L_{p0}^{W-1} L_c P_{\mathrm{in}}^{\lambda_n} \tag{6a}$$

$$P_{D\,\mathrm{cse,ON}}^{\lambda_n} = L_{p0}^{2(n-1)} L_{p1} P_{\mathrm{in}}^{\lambda_n}. \tag{6b}$$

Considering the CSE in the OFF state, the output powers at the through, drop, and add ports for an input optical signal carried on the wavelength λ_n is calculated in (7). As can be seen from (6) and (7), the analytical models for the CSE are based on the analyses of the PSE and waveguide crossing. For example, the output power at the through port of the CSE in the ON state is associated with the passing loss of the PSE in the ON state, $P_{T\,\mathrm{pse,ON}}$ defined in (4a), and the crossing loss in the waveguide crossing, P_{Out1} calculated in (1a). It is worth mentioning that $P_{A\,\mathrm{cse,ON}} = P_{R\,\mathrm{cse,ON}} = P_{R\,\mathrm{cse,OFF}} = 0$ since the first-order incoherent crosstalk noise is considered. In addition, for simplification, the bending loss between the add and drop ports is not considered

$$P_{T\,\mathrm{cse,OFF}}^{\lambda_n} = L_{p0}^{W} L_c P_{\mathrm{in}}^{\lambda_n} \tag{7a}$$

$$P_{D\,\mathrm{cse,OFF}}^{\lambda_n} = K_{p0} L_{p0}^{2(n-1)} P_{\mathrm{in}}^{\lambda_n} + \sum_{j=1, j\neq n}^{W} \left(L_{p0}^{2(j-1)} \psi\left(n, \lambda'_{\mathrm{MR}\,j}\right) \right) P_{\mathrm{in}}^{\lambda_n} + L_{p0}^{W} K_c P_{\mathrm{in}}^{\lambda_n} \tag{7b}$$

$$P_{A\,\mathrm{cse,OFF}}^{\lambda_n} = L_{p0}^{W} K_c P_{\mathrm{in}}^{\lambda_n}. \tag{7c}$$

The optical modulator structure, as a part of the E-O interface, is shown in Fig. 2(a) in which it is assumed that no crossing exists between the waveguides transmitting power and the one carrying data. We carefully studied different possible modulation structures, and the one shown in Fig. 2 resulted in low crosstalk noise by separating different optical wavelengths at the modulation and switching stages before the out port. The optical signal of the wavelength λ_n is generated at its corresponding VCSEL, VCSEL λ_n, then is modulated at the modulator M_n, and finally is directed to the communication line toward the out port through the MR n. The power of the optical signal carried on the wavelength λ_n at the out port in the optical modulator is calculated in (8). In this equation, P_v is the optical signal power at the VCSEL and L_m is the average modulation loss at the modulator. In this paper, we assume that $L_m = L_{p0}$

$$P_{\mathrm{Msignal}}^{\lambda_n} = L_m L_{p0}^{W-n} L_b^2 L_{p1} P_v^{\lambda_n}. \tag{8}$$

Fig. 2(b) shows the photodetector structure as a part of the O-E interface. The optical signal of the wavelength λ_n couples into the MR n and then is directed to the photodetector n, PD_n. When the power of the optical signal on the wavelength λ_n at the input port of the photodetector equals $P_{\mathrm{in}}^{\lambda_n}$, (9a) defines the signal power received at the photodetector n, $P_{\mathrm{Dsignal}}^{\lambda_n}$, while (9b) calculates the crosstalk noise from the optical signals on the other wavelengths

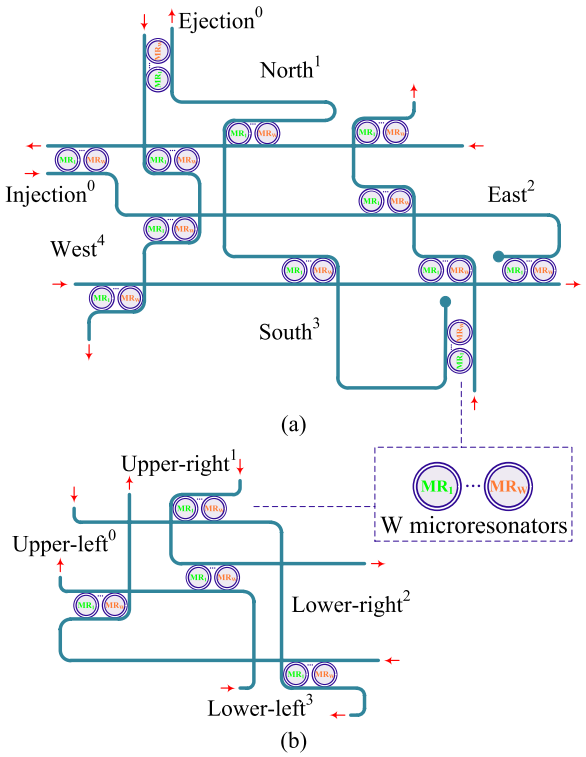

Fig. 3. (a) Crux optical router and (b) OTAR designed for WDM-based ONoCs using W optical wavelengths.

received at that photodetector, $P_{\mathrm{Dnoise}}^{\lambda_n}$. It is worth mentioning that different from Fig. 1(b), this crosstalk noise is incoherent

$$P_{\mathrm{Dsignal}}^{\lambda_n} = L_{p0}^{n-1} L_{p1} P_{\mathrm{in}}^{\lambda_n} \tag{9a}$$

$$P_{\mathrm{Dnoise}}^{\lambda_n} = L_{p0}^{(n-1)} \left(\sum_{j=n+1}^{W} \psi(j, \lambda_{\mathrm{MR}n}) \right) P_{\mathrm{in}}^{\lambda_n}. \tag{9b}$$

B. Crosstalk Noise in WDM-Based Optical Routers

Optical routers are the key components in ONoCs since they transmit information between a source and a destination processor. Different optical routers have been proposed for mesh-based, folded-torus-based, and fat-tree-based ONoCs. Fig. 3 shows the Crux optical router, which is used in mesh-based and folded-torus-based ONoCs using WDM, and the OTAR, which is designed for fat-tree-based ONoCs using WDM. Both optical routers can route optical signals on W different wavelengths. The Crux optical router has five input and five output ports. Each port is assigned with a number and can be shown as I_i, where i equals 0 for the injection/ejection, 1 for the North, 2 for the East, 3 for the South, and 4 for the West. However, the OTAR has four input and four output ports, including the upper left, upper right, lower right, and lower left ports. The numbers assigned to these ports are $i = 0$ for the upper left, $i = 1$ for the upper right, $i = 2$ for the lower right, and $i = 3$ for the lower left. The numbers assigned to the different ports in both optical routers are shown in Fig. 3. The Crux optical router is based on the dimension-ordered routing algorithm, also known as

the XY routing algorithm, while the OTAR uses the optical turnaround routing technique proposed in [4]. In the analytical equations in this paper, the subscript a is used when the Crux optical router is employed and b is considered when the OTAR is used. Furthermore, the abbreviations M, Ft, Ftr, Wtc, and Avg are used for convenience while referring to mesh, folded-torus, fat-tree, worst case, and average, respectively. It is worth mentioning that the proposed analytical models for the Crux optical router (OTAR) can be applied to any other 5×5 (4×4) optical router

$$L_{a,i,j}^{\lambda_n} = \begin{cases} S_{a,L_{i,0}}^{\lambda_n} L_p^{W_l^{\lambda_n}{}_{i,0}}, & j = 0 \\ S_{a,L_{i,j}}^{\lambda_n} L_p^{H_{M|Ft}+W_l^{\lambda_n}{}_{i,j}}, & j \neq 0 \end{cases} \quad i, jZ \in \{0,\ldots,4\}. \tag{10}$$

Utilizing the analytical models defined for the basic optical elements, we start with analyzing the power loss in the Crux optical router. $L_{a,i,j}^{\lambda_n}$, as defined in (10), is the insertion loss from the ith input port to the jth output port in the Crux optical router for an optical signal carried on the wavelength λ_n. In this equation, $S_{a,L_{i,j}}^{\lambda_n}$ indicates the switching loss that accounts for losses from passing or coupling into MRs (L_{p0} or L_{p1}), passing waveguide crossings (L_c), and passing waveguide bendings (L_b) in the optical router. Moreover, the propagation loss inside the optical router is calculated by considering the waveguide length travelled by the optical signal λ_n between the ith input port and the jth output port, $W_l^{\lambda_n}{}_{i,j}$, and the propagation loss, L_p (Table I). We integrate the propagation loss at the network level into our optical router model: when the output port is not the ejection, $j \neq 0$, we consider the propagation loss of the waveguide that connects the optical router to the next one, as shown in (10). $H_{M|Ft}$ is the hop length and can be calculated based on $H_{M|Ft} \cong (S/M \times N)^{1/2}$ in homogeneous symmetrical mesh-based and folded-torus-based ONoCs. S is the chip size in cm^2, and $M \times N$ is the network size

$$L_{b,i,j}^{\lambda_n} = \begin{cases} S_{b,L_{i,j}}^{\lambda_n} L_p^{W_l^{\lambda_n}{}_{i,j}+2H_{Ftr}}, & \text{destination} \\ S_{b,L_{i,j}}^{\lambda_n} L_p^{W_l^{\lambda_n}{}_{i,j}+H_{Ftr}}, & \text{otherwise} \end{cases} \quad i, j \in \{0,\ldots,3\}. \tag{11}$$

Similar to (10), the insertion loss imposed on the optical signal of the wavelength λ_n travelling from the ith input port toward the jth output port in the OTAR is analyzed in (11). In this equation, the propagation loss of either $L_p^{H_{Ftr}}$, when the current optical router is not the destination, or $L_p^{2H_{Ftr}}$, when the current router is the destination, is added to the propagation loss analysis at the router level. H_{Ftr} is the hop length in optimized fat-tree-based ONoCs and can be approximated using $H_{Ftr} \cong (S/R \times C)^{1/2}$, where R and C are the number of processor cores located, respectively, in a row and a column of the optimized floorplan of fat-tree-based ONoCs [22]. According to (10) and (11), it is obvious that $L_{a|b,i,j}^{\lambda_n} \neq L_{a|b,i,j}^{\lambda_e}$ and when $n \neq e$.

When an optical signal of the wavelength λ_n whose power is $P_i^{\lambda_n}$ enters the ith input port of the optical router, the power of that optical signal at the jth output port of the optical router, $P_{i,j}^{\lambda_n}$, is defined in (12). In this equation, $L_{a|b,i,j}^{\lambda_n}$ is the insertion loss from the optical router and it can be calculated using (10) and (11)

$$P_{i,j}^{\lambda_n} = P_i^{\lambda_n} L_{a|b,i,j}^{\lambda_n}. \tag{12}$$

When an optical signal of the wavelength λ_n, which we refer to as the considered optical signal, and other optical signals from other power sources carried on the same optical wavelength, which we refer to as interfering optical signals, simultaneously pass through a single optical router, crosstalk noise will be introduced to the considered optical signal from those interfering optical signals. $n_{i,j}^{\lambda_n}$, as calculated in (13), is defined as the crosstalk noise power added to the considered optical signal on the wavelength λ_n traveling from the ith input port toward the jth output port in the optical router

$$n_{i,j}^{\lambda_n} = \sum_{m=0}^{prt\_\text{num}} \left(P_m^{\lambda_n} L_{m,j}^{\lambda_n} X_{i,j,m}^{\lambda_n} + \sum_{e=1,e\neq n}^{W} \left(P_m^{\lambda_n} L_{m,j}^{\lambda_n} Y_{i,j,m}^{e} \right) \right) \tag{13}$$

where

$$Y_{i,j,m}^{e} \equiv \psi(n, \lambda_{\text{MR}e} | \lambda'_{\text{MR}e}).$$

In this equation, $X_{i,j,m}^{\lambda_n}$ is the crosstalk noise coefficient introduced by the interfering optical signals of the wavelength λ_n, which are entering the optical router through the input port m, to the considered optical signal through the waveguide crossings and MRs associated with λ_n, i.e., MR_n. Moreover, $Y_{i,j,m}^{e}$, which is associated with $\psi(n, \lambda_{\text{MR}e} | \lambda'_{\text{MR}e})$, is the crosstalk noise coefficient from the interfering optical signals of the wavelength λ_n, but through MRs MR_e and $e \neq n$. P_m is the power of the interfering optical signal at the input port m, and $L_{m,j}$ is the insertion loss from the mth input port to the jth output port excluding the loss of the element at which the interfering optical signal mixes with the considered optical signal. In this equation, $prt\_\text{num} = 4$ when the Crux optical router is used and $prt\_\text{num} = 3$ when the OTAR is considered

$$\text{SNR}^{\lambda_n} = 10\log\left(\frac{P_S^{\lambda_n}}{P_N^{\lambda_n}}\right). \tag{14}$$

The SNR of the optical signal carried on the wavelength λ_n is defined as the ratio of the signal power to the power of the crosstalk noise corrupting the signal, as described in (14), where $P_S^{\lambda_n}$ is the optical signal power and $P_N^{\lambda_n}$ is the crosstalk noise power received at the photodetector PD_n in the receiver.

Utilizing the analytical models proposed in this section, we present an example of the OTAR in Fig. 4 to indicate how to analyze the crosstalk noise and power loss at the optical router level. We consider the use of two wavelengths ($W = 2$), λ_1 and λ_2, in this example, and we present the analyses for the optical signal on the wavelength λ_2. In the figure, the considered optical signals of the wavelengths λ_1 and λ_2 (shown in red) are travelling from the upper right input port toward the lower right output port, $i = 1$ and $j = 2$, while there are two other interfering optical signals carried

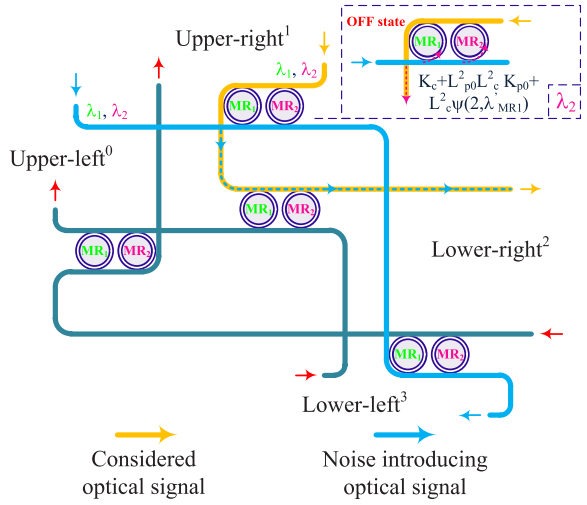

Fig. 4. Example of interference between two optical signals in the OTAR ($W = 2$).

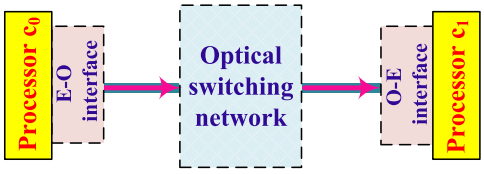

Fig. 5. Abstract overview of an optical communication between processors c_0 and c_1 in WDM-based ONoCs.

on the same wavelengths (shown in blue) travelling from the upper left input port to the lower left output port, $m = 0$, and they mix with the considered optical signals through the CSE shown in the figure. There are other possible interfering optical signals from other input ports, and those from the upper left to the lower left ports are indicated as an example. Employing (11) and (12), the signal power at the lower right output port is $P^{\lambda_2}_{1,2} = P^{\lambda_2}_1 L^{\lambda_2}_{b,1,2} = P^{\lambda_2}_1 L^2_b L^4_{p0} L^2_c$, in which $P^{\lambda_2}_1$ is the power of the optical signal carried on the wavelength λ_2 at the upper right input port. Considering (13), the crosstalk noise power added to the considered optical signal on the wavelength λ_2, $n^{\lambda_2}_{1,2}$, and received at the lower right output port is defined in

$$\begin{aligned} n^{\lambda_2}_{1,2} &= P^{\lambda_2}_0 L^{\lambda_2}_{b,0,2}\left(X^{\lambda_2}_{1,2,0} + Y^1_{1,2,0}\right) \\ &= P^{\lambda_2}_0 L^2_b L^2_{p0} L^2_c \left(\left(K_c + L^2_{p0} L^2_c K_{p0}\right) + L^2_c \psi\left(2, \lambda'_{\mathrm{MR}\,1}\right)\right). \end{aligned} \tag{15}$$

The SNR at the lower right output port can be calculated using the received signal power and the crosstalk noise power at this port. Following the same approach defined in (15), we can calculate the total crosstalk noise power from interfering optical signals to a considered optical signal at each optical router on the considered optical link in the network.

IV. SNR in WDM-Based Optical Networks-on-Chip

Leveraging the proposed analytical models for basic photonic devices and optical routers, we present crosstalk noise and SNR analyses at the network level for WDM-based ONoCs in this section. Fig. 5 shows an overview of an on-chip optical communication in WDM-based ONoCs. When the processor core c_0 decides to communicate with another processor core c_1, optical signals of different wavelengths will be generated at off-chip VSCELs and then they will be modulated at the modulators in the E-O interface of the processor c_0. Those optical signals then pass through the optical switching network and ultimately will be received at the processor core c_1 after being detected at the photodectors in the O-E interface of that processor. All along this optical path, however, the optical signals on different wavelengths suffer from power losses and crosstalk noise will also be accumulated on them. When an optical signal carried on the wavelength λ_n travels from the processor core c_0 toward the core c_1, the signal power received at the latter core can be calculated based on

$$\mathrm{PL}^{\lambda_n}_{(c_0,c_1)} = P^{\lambda_n}_v L^{\lambda_n}_{\mathrm{Mod}} L^{\lambda_n}_{(c_0,c_1)\mathrm{Net}} L^{\lambda_n}_{\mathrm{Det}}. \tag{16}$$

In this equation, $P^{\lambda_n}_v$ is the optical power at the VCSEL n generating an optical signal on the wavelength λ_n. Moreover, $L^{\lambda_n}_{\mathrm{Mod}}$ and $L^{\lambda_n}_{\mathrm{Det}}$, can be calculated based on (8) and (9a), and are, respectively, the modulation loss and detection loss imposed on the optical signal of the wavelength λ_n, while $L^{\lambda_n}_{(c_0,c_1)\mathrm{Net}}$ denotes the power loss from passing the optical routers in the optical switching network, and it can be calculated using (10) and (11). The subscript Net varies based on the ONoC architecture in use, and it can be M, Ft, or Ftr when considering mesh-based, folded-torus-based, or fat-tree-based ONoCs, respectively. While $L^{\lambda_n}_{\mathrm{Mod}}$ and $L^{\lambda_n}_{\mathrm{Det}}$ are the same for different WDM-based ONoCs in this paper, $L^{\lambda_n}_{(c_0,c_1)\mathrm{Net}}$ relies on the topological properties of each ONoC architecture and hence is different in various WDM-based ONoCs.

The crosstalk noise from the interfering optical signals accumulated on the considered optical signal of the wavelength λ_n while it is travelling from the processor core c_0 toward the core c_1 is calculated in

$$N^{\lambda_n}_{(c_0,c_1)} = N^{\lambda_n}_{\mathrm{Mod}} + N^{\lambda_n}_{(c_0,c_1)\mathrm{Net}} + N^{\lambda_n}_{\mathrm{Det}}. \tag{17}$$

In this equation, $N^{\lambda_n}_{\mathrm{Mod}}$ and $N^{\lambda_n}_{\mathrm{Det}}$, defined in (9b), show the crosstalk noise power from the modulator and detector, respectively. Furthermore, $N^{\lambda_n}_{(c_0,c_1)\mathrm{Net}}$ is the crosstalk noise introduced to the optical signal on the wavelength λ_n through the optical routers inside the optical switching network. We assume that $N_{\mathrm{Mod}} \cong 0$ since the amount of crosstalk noise from the modulators at the receiver side is negligible. $N^{\lambda_n}_{\mathrm{Det}}$ is the same in different WDM-based ONoCs, but analyzing $N^{\lambda_n}_{(c_0,c_1)\mathrm{Net}}$ depends on each ONoC architecture. In this section, an effort is made to systematically analyze the worst case as well as the average $L^{\lambda_n}_{(c_0,c_1)\mathrm{Net}}$ and $N^{\lambda_n}_{(c_0,c_1)\mathrm{Net}}$ in the three well-known ONoC architectures, mesh-based, folded-torus-based, and fat-tree-based ONoCs using WDM.

Figs. 6 and 7, respectively, show $M \times N$ WDM-based mesh-based and folded-torus-based ONoCs, and the optimized WDM-based fat-tree-based ONoC comprises k processor cores. In these figures, the optical signals of different wavelengths are shown using a single optical signal for convenience. As Fig. 7 shows, when the number of processor

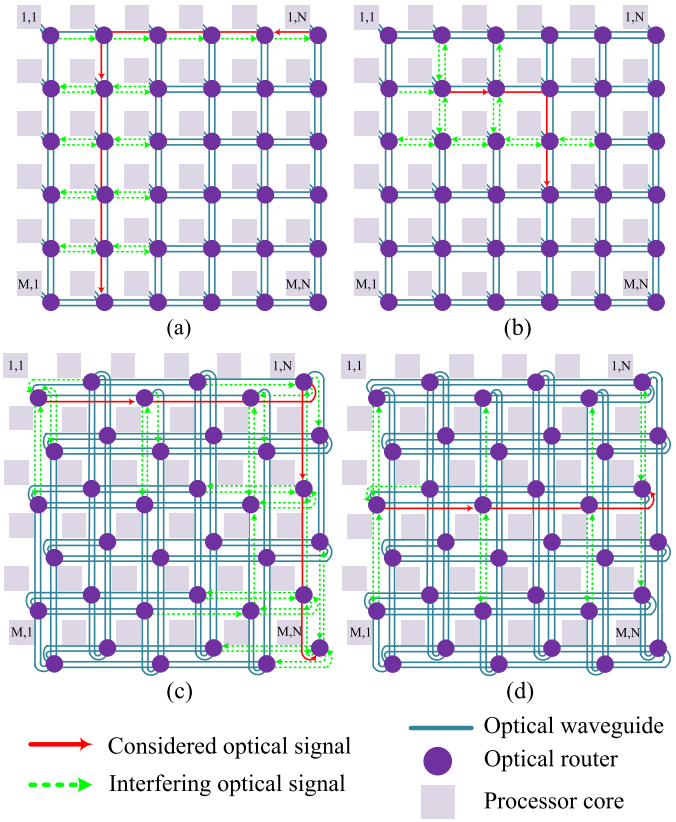

Fig. 6. (a) and (c) Worst case and (b) and (d) average SNR optical links in $M \times N$ WDM-based mesh-based and folded-torus-based ONoCs using the Crux optical router and W wavelengths.

cores is equal to k, there are a total number of $\log_2 k - 1$ levels in the fat tree. Each level is assigned with a number, and we assume that the processor cores are located at level 0 and are connected to the optical routers at level 1. Optical routers at different levels are illustrated in different colors for convenience. The diverse architectural properties of the three ONoC architectures result in different worst case and average analyses, as we will show in this section.

The worst case SNR link simultaneously suffers from high-power loss and crosstalk noise. Compared with the worst case SNR link, the average SNR link passes through a smaller number of optical routers, the average hop length in this case, and suffers from less crosstalk noise compared with the worst case link. In the following, we systematically analyze the worst case and the average crosstalk noise and SNR in WDM-based ONoCs. In this paper, M and N are supposed to be even numbers.

A. Worst Case Analyses

Worst case SNR analyses in mesh-based, folded-torus-based, and fat-tree-based ONoCs using the single-wavelength approach were proposed in [6]–[8]. Based on the analyses' results from those previous works, we have analyzed different optical links among the longest in WDM-based ONoCs and have found that the worst case SNR optical links, i.e., the routing paths inside the optical switching network, in mesh-based, folded-torus-based, and fat-tree-based ONoCs using WDM are similar to those demonstrated in those previous

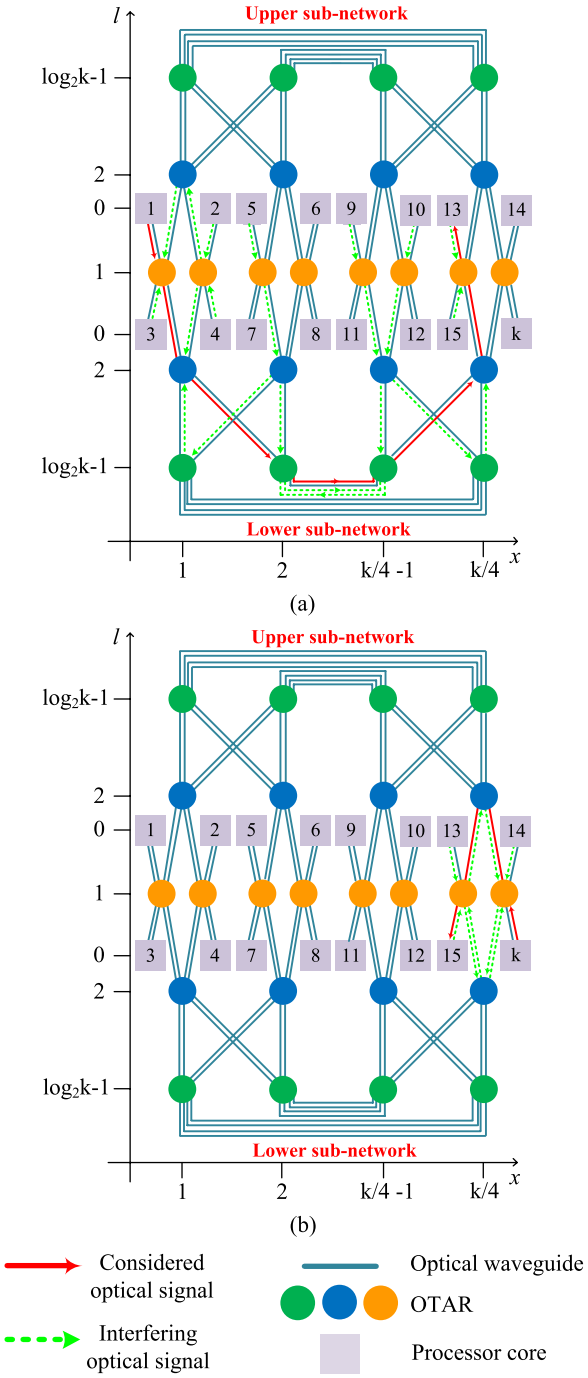

Fig. 7. (a) Worst case and (b) average SNR optical links in WDM-based fat-tree-based ONoCs using the OTAR and W wavelengths.

works. Considering (16) and (17), one can note that the power loss and crosstalk noise caused by the modulation and detection are unique among different optical links (routing paths). However, the power loss and crosstalk noise from the optical switching network depend on the routing path as well as the ONoC architecture under study, as also discussed above (Fig. 5). Therefore, the worst case routing path and the communication pattern that introduces the highest crosstalk noise to the worst case SNR link inside the optical switching network in each WDM-based ONoC architecture remain the same as those in a single-wavelength-based ONoC. Nevertheless, when using the WDM, the analyses and results

are different due to the presence of different optical wavelengths. In this subsection, we present the worst case crosstalk noise and SNR analyses for WDM-based folded-torus-based ONoCs. The worst case SNR analysis for the other two WDM-based ONoC architectures, shown in Figs. 6(a) and 7(a), is based on the worst case SNR analyses in [6] and [8] and follows the same analytical approach proposed for WDM-based folded-torus-based ONoCs.

We previously demonstrated that the worst case SNR link in folded-torus-based ONoCs using the single-wavelength approach and an arbitrary 5×5 optical router should be among the first, second, third, and fourth longest optical links [7]. We have analyzed the SNR of those optical links in WDM-based folded-torus-based ONoCs using the Crux optical router to find the worst case SNR link. The analyses' results indicate that when the Crux optical router is employed the optical link from the processor core (1, 1) toward the core *(M, N)*, as shown in Fig. 6(c), has the worst case SNR. Considering all the possible traffic patterns and dynamic workloads in the network, the communication pattern, shown as dotted-green lines in Figs. 6 and 7, is considered in such a way as to guarantee that the worst case (average) crosstalk noise be received at the destination of the optical signal while analyzing the worst case (average) SNR in each architecture. According to Fig. 6(c) and (16), the power of the optical signal of the wavelength λ_n on the worst case SNR link in WDM-based folded-torus-based ONoCs using the Crux optical router is calculated in (18a), and the worst case power loss from the optical switching network, $WtcL^{\lambda_n}_{((1,1),(M,N))_{Ft}}$, is defined in (18b). The seven terms on the right-hand side of the latter equation represent the insertion losses from the optical routers on the path (first five terms), the crossing loss from the waveguide crossings at the network level, and the bending losses. The first subscript, a, indicates the use of the Crux optical router, while the second and third subscripts represent, respectively, the input and output port numbers in the optical router (Fig. 3)

$$WtcPL^{\lambda_n}_{((1,1),(M,N))} = P^{\lambda_n}_{v} L^{\lambda_n}_{\text{Mod}} WtcL^{\lambda_n}_{((1,1),(M,N))_{Ft}} L^{\lambda_n}_{\text{Det}} \tag{18a}$$

where

$$WtcL^{\lambda_n}_{((1,1),(M,N))_{Ft}} = L^{\lambda_n}_{a,0,2} L^{\lambda_n\left(\frac{N}{2}-1\right)}_{a,4,2} L^{\lambda_n}_{a,2,3} L^{\lambda_n\left(\frac{M}{2}-1\right)}_{a,1,3} L^{\lambda_n}_{a,3,0} L_c^{3M+3N-4} L_b^2. \tag{18b}$$

In (18b), the insertion losses imposed by passing an optical router can be calculated based on (10). By way of example, according to the Crux optical router structure in Fig. 3(a) and using (10), $L^{\lambda_n}_{a,0,2}$, i.e., the insertion loss from the injection port toward the East output port for the optical signal on the wavelength λ_n, equals $L^{5W-2n}_{p0} L_{p1} L_b^4 L_c^3$.

Considering the worst case SNR link shown in Fig. 6(c), the worst case crosstalk noise power accumulated on the optical signal carried on the wavelength λ_n on that link is calculated in

$$WtcN^{\lambda_n}_{((1,1),(M,N))} = WtcN^{\lambda_n}_{((1,1),(M,N))_{Ft}} + N^{\lambda_n}_{\text{Det}} \tag{19a}$$

where

$$WtcN^{\lambda_n}_{((1,1),(M,N))_{Ft}} = n^{\lambda_n}_{a,0,2} + \left(\frac{N}{2}-1\right) n^{\lambda_n}_{a,4,2} + n^{\lambda_n}_{a,2,3} + \left(\frac{M}{2}-1\right) n^{\lambda_n}_{a,1,3} + n^{\lambda_n}_{a,3,0}. \tag{19b}$$

In this equation, $WtcN^{\lambda_n}_{((1,1),(M,N))_{Ft}}$ is the worst case crosstalk noise power accumulated on the optical signal λ_n on the worst case SNR link through the optical switching network, and it is defined in (19b). In this equation, $n^{\lambda_n}_{i,j}$, as defined in (13), is the crosstalk noise power added to the considered optical signal of the wavelength λ_n. Different $n^{\lambda_n}_{i,j}$ can be defined similarly to the crosstalk noise power calculation in (15) proposed for the example shown in Fig. 4. The power of the interfering optical signals at each Crux optical router on the worst case SNR link can be calculated based on the communication pattern shown in Fig. 6(c). For instance, considering the first Crux optical router on the worst case SNR link indicated in this figure, the considered optical signal traveling from the injection port toward the East output port is mixed with the interfering optical signals through the North, South, and West input ports. The crosstalk noise power accumulated on the considered optical signal through these input ports can be calculated using $n^{\lambda_n}_{a,0,2}$, in which the power of the interfering optical signal, for example, at the North input port, $P^{\lambda_n}_1$ in (13), equals $P^{\lambda_n}_{v} L^{\lambda_n}_{\text{Mod}} L^{\lambda_n}_{((2,1),(1,1))_{Ft}}$, where $L^{\lambda_n}_{((2,1),(1,1))_{Ft}} = L^{\lambda_n}_{a,0,1} L_b L_c^2$ [Fig. 6(c) and (16)]. Similarly, the power of the interfering optical signals at the South input port, $P^{\lambda_n}_3$, and at the West input port, $P^{\lambda_n}_4$, can be calculated.

The worst case SNR in WDM-based folded-torus-based ONoCs using the Crux optical router for the optical signal of the wavelength λ_n is calculated in

$$WtcSNR^{\lambda_n}_{((1,1),(M,N))} = 10 \log \left(\frac{WtcPL^{\lambda_n}_{((1,1),(M,N))}}{WtcN^{\lambda_n}_{((1,1),(M,N))}} \right). \tag{20}$$

In this equation, $WtcPL^{\lambda_n}_{((1,1),(M,N))}$ is the detected optical signal power carried on the wavelength λ_n on the worst case SNR link and is defined in (18a), while $WtcN^{\lambda_n}_{((1,1),(M,N))}$, defined in (19a), denotes the worst case crosstalk noise power received at the photodetector PD_n associated with the optical signal λ_n in the receiver.

B. Average Analyses

The signal power loss is associated with the hop length of the signal, and hence the average hop length needs to be considered to analyze the average signal power loss in each ONoC architecture. Moreover, the crosstalk noise introduced by the average SNR link and the other interfering optical links should result in the average crosstalk noise power being received at the destination of the average SNR link. While the power loss and crosstalk noise analyses for the modulation and detection are the same as those proposed for the worst case analyses, the average power loss and crosstalk noise power from the optical switching network in the average case

is different. Given the network size is $M \times N$, (21a) indicates the average hop length in mesh-based ONoCs, H_{Avg_M}, while the average hop length in folded-torus-based ONoCs, $H_{\text{Avg}_{Ft}}$, when M and N are even numbers, is calculated in (21b) [23]. In addition, the average hop length in optimized fat-tree-based ONoCs consisting of k processor cores is defined in (21c)

$$H_{\text{Avg}_M} = \left\lfloor \frac{M+N}{3} \right\rfloor \tag{21a}$$

$$H_{\text{Avg}_{Ft}} = \left\lfloor \frac{(M^2+2M)(N+1)+(N^2+2N)(M+1)}{4(MN+M+N)} \right\rfloor \tag{21b}$$

$$H_{\text{Avg}_{Ftr}} = \left\lceil \sum_{i=2}^{\log_2 k-1} \left(\frac{1}{2^{i-1}} (\log_2 k - i - 1) \right) + \log_2 k - \frac{1}{2} \right\rceil. \tag{21c}$$

We have analyzed different optical links with the average hop length in WDM-based mesh-based and folded-torus-based ONoCs using the Crux optical router as well as in WDM-based fat-tree-based ONoCs using the OTAR, and we have found that the optical links shown in Figs. 6(b) and (d), and 7(b) are the average SNR links in those ONoC architectures, respectively.

The average SNR link in WDM-based mesh-based ONoCs using the Crux optical router is the one that starts from the processor core $c_0 = (2, 2)$, passes through $\alpha_1 = \lfloor N/3 \rfloor - 1$ routers on the X-section, turns to the Y-section, passes through $\alpha_2 = \lfloor M/3 \rfloor - 1 + (\lfloor M + N/3 \rfloor \text{mod} 2)$ routers on the Y-section, and finally is received at its destination core, c_1, as shown in Fig. 6(b). Using (21a) and (16), the power loss imposed on the optical signal of the wavelength λ_n on this link is calculated in (22a). Since the average SNR link is diverse for different network sizes, we use c_1 to indicate the destination of the average SNR link in each ONoC. For each network size, c_1 can be determined by considering the coordinates of the source processor core, the optical path shown in Figs. 6(b) and (d), and 7(b), and is based on the average hop length for each ONoC architecture

$$\text{Avg}PL^{\lambda_n}_{((2,2),c_1)} = P^{\lambda_n}_{v} L^{\lambda_n}_{\text{Mod}} \text{Avg}L^{\lambda_n}_{((2,2),c_1)_M} L^{\lambda_n}_{\text{Det}} \tag{22a}$$

where

$$\text{Avg}L^{\lambda_n}_{((2,2),c_1)_M} = L^{\lambda_n}_{a,0,2} L^{\lambda_n(\alpha_1)}_{a,4,2} L^{\lambda_n}_{a,4,3} L^{\lambda_n(\alpha_2)}_{a,1,3} L^{\lambda_n}_{a,1,0}. \tag{22b}$$

In (22a), $\text{Avg}L^{\lambda_n}_{((2,2),c_1)_M}$ is the power loss imposed on the average SNR link through the optical switching network, as defined in (22b). Considering the communication pattern shown in Fig. 6(b), the average crosstalk noise power introduced by the interfering optical signals to the considered optical signal of the wavelength λ_n on the average SNR link is calculated in

$$\text{Avg}N^{\lambda_n}_{((2,2),c_1)} = \text{Avg}N^{\lambda_n}_{((2,2),c_1)_M} + N^{\lambda_n}_{\text{Det}} \tag{23a}$$

where

$$N^{\lambda_n}_{((2,2),c_1)_M} = n^{\lambda_n}_{a,0,2} + \alpha_1 n^{\lambda_n}_{a,4,2} + n^{\lambda_n}_{a,4,3} + \alpha_2 n^{\lambda_n}_{a,1,3} + n^{\lambda_n}_{a,1,0}. \tag{23b}$$

Considering the average signal power, defined in (22a), and the average crosstalk noise power, calculated in (23a), the average SNR at the destination of the optical signal on the wavelength λ_n in WDM-based mesh-based ONoCs using the Crux optical router can be calculated using

$$\text{AvgSNR}^{\lambda_n}_{((2,2),c_1)} = 10 \log \left(\frac{\text{Avg}PL^{\lambda_n}_{((2,2),c_1)}}{\text{Avg}N^{\lambda_n}_{((2,2),c_1)}} \right). \tag{24}$$

Fig. 6(d) shows the average SNR link in WDM-based folded-torus-based ONoCs using the Crux optical router. Similar to the average analyses proposed for WDM-based mesh-based ONoCs, the average signal power, crosstalk noise power, and SNR in WDM-based folded-torus-based ONoCs using the Crux optical router are calculated in

$$\text{PL}^{\lambda_n}_{((3,1),c_1)} = P^{\lambda_n}_{v} L^{\lambda_n}_{\text{Mod}} \text{Avg}L^{\lambda_n}_{((3,1),c_1)_{Ft}} L^{\lambda_n}_{\text{Det}} \tag{25a}$$

where

$$\text{Avg}L^{\lambda_n}_{((3,1),c_1)_{Ft}} = L^{\lambda_n}_{a,0,2} L^{\lambda_n(\lfloor \frac{N+1}{2} \rfloor - 1)}_{a,4,2} L^{\lambda_n}_{a,2,0} L_c^{6\lfloor \frac{N+1}{2} \rfloor - 2} L_b \tag{25b}$$

$$\text{Avg}N^{\lambda_n}_{((3,1,),c_1)} = \text{Avg}N^{\lambda_n}_{((3,1),c_1)_{Ft}} + N^{\lambda_n}_{\text{Det}} \tag{26a}$$

where

$$\text{Avg}N^{\lambda_n}_{((3,1),c_1)_{Ft}} = n^{\lambda_n}_{a,0,2} + \left(\left\lfloor \frac{N+1}{2} \right\rfloor - 1 \right) n^{\lambda_n}_{a,4,2} + n^{\lambda_n}_{a,2,0} \tag{26b}$$

$$\text{AvgSNR}^{\lambda_n}_{((3,1),c_1)} = 10 \log \left(\frac{\text{AvgPL}^{\lambda_n}_{((3,1),c_1)}}{\text{Avg}N^{\lambda_n}_{((3,1),c_1)}} \right). \tag{27}$$

Moreover, the average signal power, crosstalk noise power, and SNR in WDM-based fat-tree-based ONoCs using the OTAR, shown in Fig. 7(b), can be calculated based on

$$\text{AvgPL}^{\lambda_n}_{(k,c_1)} = P^{\lambda_n}_{v} L^{\lambda_n}_{\text{Mod}} \text{Avg}L^{\lambda_n}_{(k,c_1)_{Ftr}} L^{\lambda_n}_{\text{Det}} \tag{28a}$$

where

$$\text{Avg}L^{\lambda_n}_{(k,c_1)_{Ftr}} = L^{\lambda_n(2)}_{b,3,1} L^{\lambda_n(\log_2 k-5)}_{b,2,1} L_{b,2,3} L^{\lambda_n(\log_2 k-5)}_{b,1,2} L^{\lambda_n}_{b,1,3} L_b^{\alpha_3} L_c^{\alpha_4} \tag{28b}$$

$$\text{Avg}N^{\lambda_n}_{(k,c_1)} = \text{Avg}N^{\lambda_n}_{(k,c_1)_{Ftr}} + N^{\lambda_n}_{\text{Det}} \tag{29a}$$

where

$$\text{Avg}N^{\lambda_n}_{(k,c_1)_{Ftr}} = 2n^{\lambda_n}_{b,3,1} + (\log_2 k - 5) n^{\lambda_n}_{b,2,1} + n_{b,2,3} + (\log_2 k - 5) n^{\lambda_n}_{b,1,2} + n^{\lambda_n}_{b,1,3} \tag{29b}$$

$$\text{AvgSNR}^{\lambda_n}_{(k,c_1)} = 10 \log \left(\frac{\text{AvgPL}^{\lambda_n}_{(k,c_1)}}{\text{Avg}N^{\lambda_n}_{(k,c_1)}} \right). \tag{30}$$

In these equations, $\alpha_3 = 4 \log_2 k - 10$ and $\alpha_4 = 2^{(\log_2 k-3)} - 2$. In addition, the subscript k represents the source processor core's number.

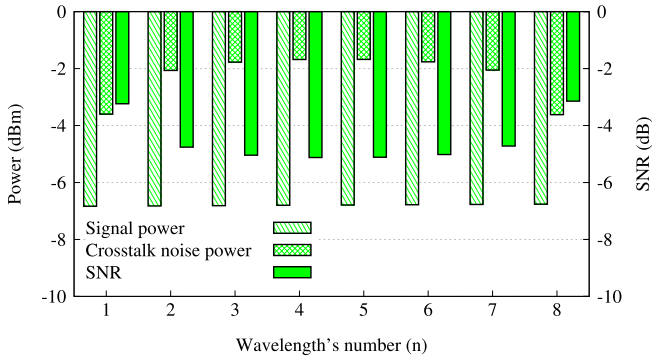

Fig. 8. Worst case signal power, crosstalk noise power, and SNR in an 8×8 WDM-based mesh-based ONoC using the Crux optical router ($W = 8$, FSR $= 6$ nm, and $Q = 9000$).

V. Quantitative Simulations

The proposed analytical models for the worst case as well as the average crosstalk noise and SNR in different WDM-based ONoC architectures have been included in our newly developed CLAP [7], [24]. Using CLAP and applying recent fabricated device parameters, as listed in Table I, we present and compare the quantitative simulation results of the worst case as well as the average signal power, crosstalk noise power, and SNR in real case studies of WDM-based mesh-based, folded-torus-based, and fat-tree-based ONoCs using the Crux optical router and the OTAR. It is assumed that the injection laser power, P_v, at the different VCSELs is the same and is equal to 0 dBm. It is worth mentioning that the output power at the E-O interface depends on the power loss imposed on the optical path. Moreover, a waveguide with a size of 450 nm $\times$ 200 nm and an MR with a diameter of 10 μm are considered.

Fig. 8 shows the worst case signal power, crosstalk noise power, and SNR received at different photodetectors at the destination of the worst case SNR link in an 8×8 mesh-based ONoC using the Crux optical router [Fig. 6(a)] when W, FSR, and Q equal 8, 6 nm, and 9000, respectively. As can be seen, while the signal power slightly decreases as the wavelength's number, n, increases, the crosstalk noise power rises when $n < (W/2)$, peaks at $n = (W/2)$, and then moderately reduces for $n > (W/2)$. Accordingly, the SNR decreases at first and then starts increasing for the last few wavelengths. The behavior of the crosstalk noise power can be described based on (3b): when $|\lambda_n - \lambda_{\mathrm{MR}m}|$ is larger, the resulting crosstalk noise power will be lower, and as it declines, the crosstalk noise power will become higher. Since the results for different wavelengths are not the same, we consider the worst case (average) values among different wavelengths when showing the worst case (average) results in the rest of this paper.

The proposed analytical models for WDM-based ONoCs in Section IV are based on W, FSR, and Q. Understanding the SNR variations based on employing different values for those parameters, we analyze and compare the worst case SNR in different ONoC architectures of the same network size ($M = N = 8$ and $k = 64$) while considering different values of W, FSR, and Q in CLAP. The analyses' results from CLAP are shown in Fig. 9, in which we consider

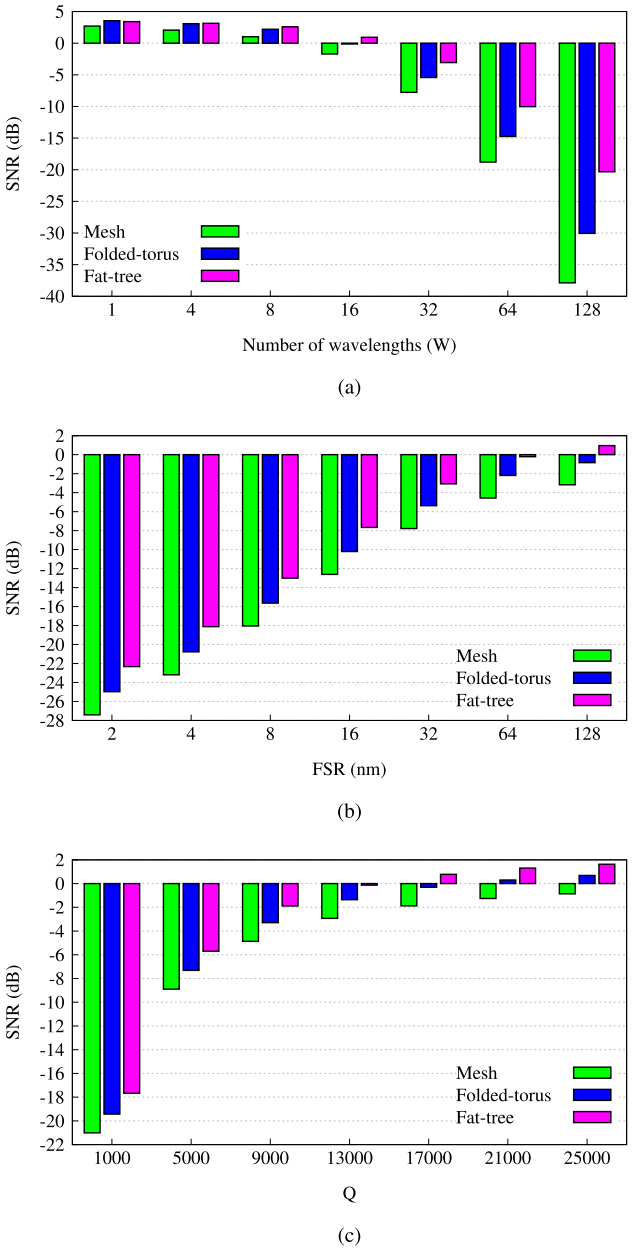

Fig. 9. Worst case SNR in 8×8 (64-core) WDM-based mesh-based, folded-torus-based, and fat-tree-based ONoCs using the Crux optical router and OTAR while considering different values of W, FSR, and Q. (a) FSR $= 32$ nm and $Q = 9000$. (b) $W = 32$ and $Q = 9000$. (c) $W = 16$ and FSR $= 32$ nm.

using $\epsilon = (\mathrm{FSR}/2W)$. It is worth mentioning that the MRs diameter varies according to the employed values of Q and FSR in Fig. 9. As Fig. 9(a) shows, when the FSR and Q are, respectively, 32 nm and 9000 and W varies, the SNR decreases with an increase in W. In other words, when W increases, a larger number of MRs is required, which imposes a higher power loss and crosstalk noise power, and hence a lower SNR. In addition, as W increases over a fixed FSR, the spacing among different wavelengths becomes smaller, which results in a higher crosstalk noise power, and consequently lower SNR. Fig. 9(b) shows the SNR variations when $W = 32$ and $Q = 9000$, but FSR varies from 2 to 128 nm. As the FSR increases, the spacing among different optical

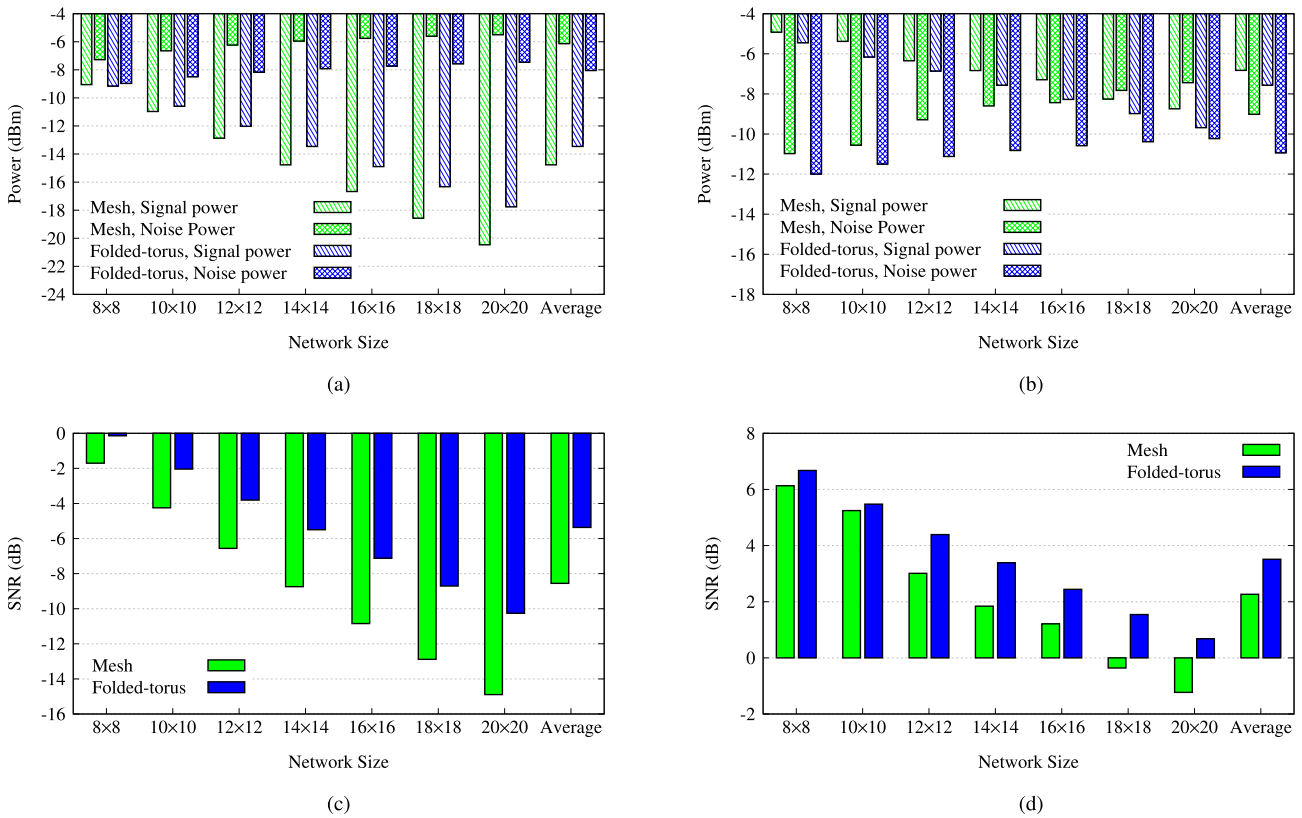

Fig. 10. Signal power, crosstalk noise power, and SNR in WDM-based mesh-based and folded-torus-based ONoCs using the Crux optical router ($W = 16$, FSR $= 32$ nm, and $Q = 9000$). (a) Worst case signal and crosstalk noise power. (b) Average signal and crosstalk noise power. (c) Worst case SNR. (d) Average SNR.

wavelengths becomes larger, and thus the SNR improves [see (3b)]. Considering Fig. 9(a) and (b), one can notice that when $Q = 9000$ and $(\text{FSR}/W) > 1$ nm, the resultant SNR is improved. However, $(\text{FSR}/W) \gg 1$ nm cannot considerably improve the SNR. Finally, Fig. 9(c) shows the SNR variations under different values of Q and when $W = 16$ and FSR $= 32$ nm. The higher the value of Q, the better the SNR is. Furthermore, there is a slight improvement in the SNR when Q becomes very large.

Fig. 10 shows the worst case and the average signal power, crosstalk noise power, and SNR comparison between WDM-based mesh-based and folded-torus-based ONoCs using the Crux optical router under different network sizes. We considered the use of 16 wavelengths, $W = 16$, with FSR $= 32$ nm and $Q = 9000$, and we found that when M and N are equal, the resulting SNR is the best. Hence, in the simulation, as shown on the x-axis in Fig. 10, we considered $M = N$. As Fig. 10(a) and (b) shows, the worst case and the average signal power decrease when the network size increases, while the worst case and the average crosstalk noise power increase. Furthermore, WDM-based folded-torus-based ONoCs have higher worst case signal power and lower crosstalk noise power compared with WDM-based mesh-based ONoCs. However, both the average signal power and crosstalk noise power in WDM-based mesh-based ONoCs are higher than those in WDM-based folded-torus-based ONoCs under different networks sizes. According to Fig. 10(c) and (d), the worst case and the average SNR exponentially reduce when the network scales. In addition, the worst case and the average SNR in WDM-based folded-torus-based ONoCs are higher than those in WDM-based mesh-based ONoCs using the Crux optical router. Another important observation is that under all the network sizes in both ONoC architectures, the worst case crosstalk noise power is higher than the signal power, and hence the worst case SNR is smaller than 0 dB. Considering the average case, however, the average crosstalk noise power only exceeds the average signal power in WDM-based mesh-based ONoCs larger than 16×16 and in folded-torus-based ONoCs larger than 20×20.

The worst case and the average signal power, crosstalk noise power, and SNR in WDM-based fat-tree-based ONoCs using the OTAR and when $W = 16$, FSR $= 32$ nm, and $Q = 9000$ are shown in Fig. 11. According to this figure, while there is a rapid reduction in the worst case and the average signal power with an increase in the number of processor cores, the worst case and the average crosstalk noise power are, respectively, almost equal to -10 and -14 dBm for different network scales. This is because when the network scales, the worst case and the average SNR link include more optical routers and this results in higher crosstalk noise accumulation and, at the same time, higher power loss. However, the accumulated crosstalk noise through a larger number of optical routers is small, and the imposed extra power loss is high enough to attenuate both the signal power and crosstalk noise power. This attenuation in signal power and the accumulated crosstalk noise power depends on the topological properties of the

TABLE II

WORST CASE AND AVERAGE SIGNAL POWER, CROSSTALK NOISE POWER, AND SNR COMPARISON ($W = 16$, FSR $= 32$ nm, AND $Q = 9000$)

Network size	Architecture	Mesh		Folded-torus		Fat-tree	
	Worst-case or Average	Worst-case	Average	Worst-case	Average	Worst-case	Average
8×8 64 cores	Signal power	-9.1 dBm	-4.9 dBm	-9.2 dBm	-5.4 dBm	-10.6 dBm	-6.4 dBm
	Crosstalk noise power	-7.3 dBm	-11 dBm	-9 dBm	-12 dBm	-11.3 dBm	-12.4 dBm
	SNR	-1.7 dB	6.1 dB	-0.1 dB	6.7 dB	0.9 dB	6.3 dB
16×16 256 cores	Signal power	-16.7 dBm	-7.3 dBm	-14.9 dBm	-8.3 dBm	-21 dBm	-8.5 dBm
	Crosstalk noise power	-5.7 dBm	-8.4 dBm	-7.7 dBm	-10.6 dBm	-11.7 dBm	-12.1 dBm
	SNR	-10.8 dB	1.2 dB	-7.1 dB	2.4 dB	-9 dB	3.9 dB

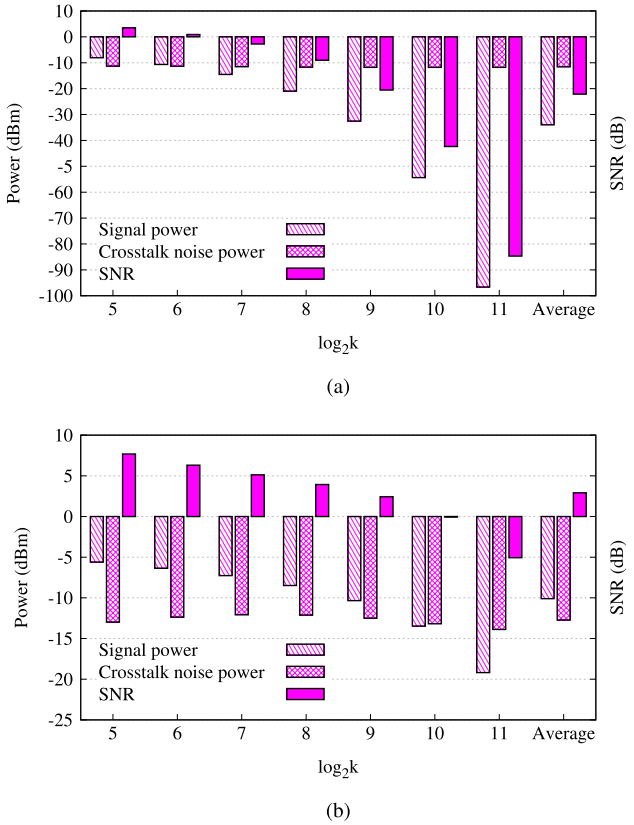

Fig. 11. Signal power, crosstalk noise power, and SNR in WDM-based fat-tree-based ONoCs using the OTAR ($W = 16$, FSR $= 32$ nm, and $Q = 9000$). (a) Worst case results. (b) Average results.

ONoC architecture and the structure of the optical router. As Fig. 11(a) shows, the worst case signal power is smaller than the worst case crosstalk noise power when the number of processor cores is larger than 2^6. In addition, considering Fig. 11(b), the average crosstalk noise power exceeds the average signal power when the number of processor cores is larger than 2^9.

Table II compares the worst case as well as the average signal power, crosstalk noise power, and SNR among the three ONoC architectures when the network size is 8×8 (64 cores) and 16×16 (256 cores). According to this table, WDM-based mesh-based ONoCs using the Crux optical router have the lowest worst case and average SNR under both network sizes. Using the same optical router and when the network size is small, WDM-based folded-torus-based ONoCs achieve the highest average SNR, while WDM-based fat-tree-based ONoCs using the OTAR have the highest worst case SNR under the same network size. As the network scales, however, the worst case SNR in WDM-based folded-torus-based ONoCs using the Crux optical router is the highest, while WDM-based fat-tree-based ONoCs using the OTAR achieve the highest average SNR. The worst case crosstalk noise power exceeds the worst case signal power in all three architectures when the network size is 16×16. Comparing the signal power efficiency, one can notice that WDM-based mesh-based ONoCs using the Crux optical router have the best worst case and average signal power when the network size is small. As the network scales, WDM-based folded-torus-based ONoCs and WDM-based mesh-based ONoCs using the Crux optical router achieve the highest worst case and average signal power, respectively.

VI. CONCLUSION

Crosstalk noise is a critical issue for the SNR performance of WDM-based ONoCs. Evaluating the worst case as well as the average crosstalk noise and SNR in different ONoC architectures helps choose a proper ONoC architecture that can efficiently satisfy certain performance and scalability requirements. We present detailed systematical analyses and comparisons of the worst case as well as the average signal power, crosstalk noise power, and SNR in WDM-based mesh-based, folded-torus-based, and fat-tree-based ONoCs using the Crux optical router and the OTAR. The proposed analytical models are integrated into a recently released CLAP to facilitate the analyses in arbitrary WDM-based ONoCs. Performing quantitative simulations in CLAP, we indicate that different ONoC architectures result in different SNR performances. Moreover, we demonstrate how the SNR varies when employing different numbers of optical wavelengths and values of FSR and Q in WDM-based ONoCs. We also find that crosstalk noise considerably restricts the scalability of ONoCs; for example, in the worst case and considering the use of 16 optical wavelengths with FSR $=$ 32 nm and $Q = 9000$, for network sizes larger than 6×6 in WDM-based folded-torus-based and WDM-based mesh-based ONoCs using the Crux optical router and larger than 64 processor cores in WDM-based fat-tree-based ONoCs using the OTAR, the crosstalk noise power exceeds the signal power.

REFERENCES

[1] E. Bonetto, L. Chiaraviglio, D. Cuda, G. A. Gavilanes Castillo, and F. Neri, "Optical technologies can improve the energy efficiency of networks," in *Proc. 35th Eur. Conf. Opt. Commun.*, Sep. 2009, pp. 1–4.

[2] M. J. Cianchetti, J. C. Kerekes, and D. H. Albonesi, "Phastlane: A rapid transit optical routing network," in *Proc. 36th Annu. ISCA*, 2009, pp. 441–450.
[3] L. Zhang, E. E. Regentova, and X. Tan, "A 2D-torus based packet switching optical network-on-chip architecture," in *Proc. SOPO*, 2011, pp. 1–4.
[4] H. Gu, J. Xu, and W. Zhang, "A low-power fat tree-based optical network-on-chip for multiprocessor system-on-chip," in *Proc. DATE*, 2009, pp. 3–8.
[5] R. Ramaswami, K. Sivarajan, and G. Sasaki, *Optical Networks: A Practical Perspective*. San Mateo, CA, USA: Morgan Kaufmann, 2009.
[6] Y. Xie *et al.*, "Formal worst-case analysis of crosstalk noise in mesh-based optical networks-on-chip," *IEEE Trans. Very Large Scale Integr. (VLSI) Syst.*, vol. 21, no. 10, pp. 1823–1836, Oct. 2013.
[7] M. Nikdast *et al.*, "Systematic analysis of crosstalk noise in folded-torus-based optical networks-on-chip," *IEEE Trans. Comput.-Aided Design Integr. Circuits Syst.*, vol. 33, no. 3, pp. 437–450, Mar. 2014.
[8] M. Nikdast *et al.*, "Fat-tree-based optical interconnection networks under crosstalk noise constraint," *IEEE Trans. Very Large Scale Integr. (VLSI) Syst.*, to be published.
[9] L. H. K. Duong *et al.*, "A case study of signal-to-noise ratio in ring-based optical networks-on-chip," *IEEE Des. Test Comput.*, vol. 31, no. 5, pp. 55–65, Oct. 2014.
[10] F. Xu and A. W. Poon, "Silicon cross-connect filters using microring resonator coupled multimode-interference-based waveguide crossings," *Opt. Exp.*, vol. 16, no. 12, pp. 8649–8657, 2008.
[11] W. Ding, D. Tang, Y. Liu, L. Chen, and X. Sun, "Compact and low crosstalk waveguide crossing using impedance matched metamaterial," *Appl. Phys. Lett.*, vol. 96, no. 11, pp. 111114-1–111114-3, Mar. 2010.
[12] Q. Li, M. Soltani, S. Yegnanarayanan, and A. Adibi, "Design and demonstration of compact, wide bandwidth coupled-resonator filters on a silicon-on-insulator platform," *Opt. Exp.*, vol. 17, no. 4, pp. 2247–2254, 2009.
[13] Y. Xie *et al.*, "Crosstalk noise and bit error rate analysis for optical network-on-chip," in *Proc. 47th ACM/IEEE DAC*, Jun. 2010, pp. 657–660.
[14] J. Chan, G. Hendry, K. Bergman, and L. P. Carloni, "Physical-layer modeling and system-level design of chip-scale photonic interconnection networks," *IEEE Trans. Comput.-Aided Design Integr. Circuits Syst.*, vol. 30, no. 10, pp. 1507–1520, Oct. 2011.
[15] M. Mehdi Vaez and C.-T. Lea, "Strictly nonblocking directional-coupler-based switching networks under crosstalk constraint," *IEEE Trans. Commun.*, vol. 48, no. 2, pp. 316–323, Feb. 2000.
[16] B.-C. Lin and C.-T. Lea, "Crosstalk analysis for microring based optical interconnection networks," *J. Lightw. Technol.*, vol. 30, no. 15, pp. 2415–2420, Aug. 1, 2012.
[17] K. Preston, N. Sherwood-Droz, J. S. Levy, and M. Lipson, "Performance guidelines for WDM interconnects based on silicon microring resonators," in *Proc. Conf. Lasers Electro-Opt.*, May 2011, pp. 1–2.
[18] P. Dong *et al.*, "Low loss silicon waveguides for application of optical interconnects," in *Proc. IEEE Photon. Soc. Summer Topical Meeting Ser.*, Jul. 2010, pp. 191–192.
[19] F. Xia, L. Sekaric, and Y. Vlasov, "Ultracompact optical buffers on a silicon chip," *Nature Photon.*, vol. 1, no. 1, pp. 65–71, Jan. 2007.
[20] G.-R. Zhou, X. Li, and N.-N. Feng, "Design of deeply etched antireflective waveguide terminators," *IEEE J. Quantum Electron.*, vol. 39, no. 2, pp. 384–391, Feb. 2003.
[21] S. Xiao, M. H. Khan, H. Shen, and M. Qi, "Modeling and measurement of losses in silicon-on-insulator resonators and bends," *Opt. Exp.*, vol. 15, no. 17, pp. 10553–10561, Aug. 2007.
[22] Z. Wang *et al.*, "Floorplan optimization of fat-tree-based networks-on-chip for chip multiprocessors," *IEEE Trans. Comput.*, vol. 63, no. 6, pp. 1446–1459, Jun. 2014.
[23] K. Feng, Y. Ye, and J. Xu, "A formal study on topology and floorplan characteristics of mesh and torus-based optical networks-on-chip," *Microprocessors Microsyst.*, vol. 37, no. 8, pp. 941–952, Nov. 2013.
[24] (2013). *Crosstalk and Loss Analysis Platform (CLAP)*. [Online]. Available: http://www.ece.ust.hk/~eexu/,

Mahdi Nikdast (S'10–M'14) received the Ph.D. degree in electronic and computer engineering from the Hong Kong University of Science and Technology, Hong Kong, in 2013.

He is currently a Post-Doctoral Fellow with the Department of Computer and Software Engineering, Polytechnique Montreal, Montreal, QC, Canada. He has authored and co-authored more than 40 papers in refereed journals and international conference publications. His current research interests include embedded and computing systems, multiprocessor systems-on-chip, and optical/photonic interconnects.

Jiang Xu (S'02–M'07) received the Ph.D. degree from Princeton University, Princeton, NJ, USA, in 2007.

He is currently an Associate Professor with the Hong Kong University of Science and Technology, Hong Kong. He has authored and co-authored more than 70 book chapters and papers in peer-reviewed journals and international conferences. His current research interests include embedded system, optical interconnects, and HW/SW codesign.

Luan H. K. Duong is currently pursuing the Ph.D. degree in electronic and computer engineering with the Hong Kong University of Science and Technology, Hong Kong.

Xiaowen Wu (S'12) is currently a Visiting Scholar with the Mobile Computing System Laboratory, Hong Kong University of Science and Technology, Hong Kong.

Xuan Wang (S'12) is currently pursuing the Ph.D. degree in electronic and computer engineering with the Hong Kong University of Science and Technology, Hong Kong.

Zhehui Wang is currently pursuing the Ph.D. degree in electronic and computer engineering with the Hong Kong University of Science and Technology, Hong Kong.

Zhe Wang is currently pursuing the Ph.D. degree in electronic and computer engineering with the Hong Kong University of Science and Technology, Hong Kong.

Peng Yang is currently pursuing the Ph.D. degree in electronic and computer engineering with the Hong Kong University of Science and Technology, Hong Kong.

Yaoyao Ye is currently with the Shannon Laboratory, Huawei Technologies Company, Ltd., Shenzhen, China. Her current research interests include interconnect networks, systems-on-a-chip, and embedded systems.

Qinfen Hao is currently with the Shannon Laboratorty, Huawei Technologies Company, Ltd., Shenzhen, China. His current research interests include computer architectures, high-performance computers, and optical interconnects.